Supporting Information

Facile Micromolding-based Fabrication of Biopolymeric–Synthetic Hydrogel Microspheres with Controlled Structures for Improved Protein Conjugation

*Sukwon Jung and Hyunmin Yi**

Table of Contents

1. Materials and Methods
2. Core-shell Structure via Polymerization-induced Phase Separation
3. PEG-rich Core and PEG-poor Shell Domains in Microspheres
4. Chitosan–PEG Microspheres under Wet and Dry States
5. Minimal Fluorescence of Microspheres without Chitosan
6. Microspheres Fabricated with Acrylate-modified Chitosan
7. Apparent Chitosan Incorporation Ratio
8. Compatibility of Chitosan with PEGDA in Aqueous Solution
9. Negligible Biomolecular Conjugation with High PEG Content Microspheres
10. TMV Assembly with Microspheres
11. Size-selective Dual Conjugation with Core-shell Structured Microspheres
12. Effect of Sphere Size on Protein Conjugation Kinetics
13. Estimated Number of Conjugation Sites in Microspheres

1. Materials and Methods

Materials

Chitosan oligosaccharide lactate (average M_n 5 kDa, > 90% deacetylation), poly(ethylene glycol) diacrylate (PEGDA, average M_n 700 Da), 2-hydroxy-2-methylpropiophenone (photoinitiator, PI), red fluorescent dye (sulforhodamine B), phosphate buffered saline (PBS) tablets (10 mM phosphate, 2.7 mM potassium chloride, 137 mM sodium chloride, pH 7.4), and saline sodium citrate (SSC) buffer (20× concentrate, molecular biology grade) were purchased from Sigma-Aldrich (St. Louis, MO). 5-(and 6-)carboxyfluorescein succinimidyl ester (NHS–fluorescein) was purchased from Pierce Biotechnology (Rockford, IL). *Trans*-cyclooctene (TCO)–PEG_4–*N*-hydroxysuccinimide (NHS) ester, Tetrazine (Tz)–PEG_5–NHS ester, azadibenzocyclooctyne (ADIBO)–*sulfo*–NHS ester, and azide–Fluor 488 (F-488) were purchased from Click Chemistry Tools (Scottsdale, AZ). Acrylate–PEG–succinimidyl valerate (SVA) with average MW 1 kDa was purchased from Laysan Bio, Inc. (Arab, AL). NHS–PEG_{12}–azide, borate buffer (20× concentrate, 50 mM borate, pH 8.5), Tween 20 (TW20), poly(dimethylsiloxane) (PDMS) elastomer kits (Sylgard 184), and centrifugal filter units (Amicon Ultra 0.5) were purchased from Thermo Fisher Scientific (Waltham, MA). Dimethyl sulfoxide (DMSO, extra dry) and *N*-hexadecane (99%) were purchased from ACROS Organics™. 2-propanol (> 99.7%) was purchased from J.T.Baker®. All the chemicals were analytical grade, and used without further purification.

DNA Oligonucleotides and Proteins

All single-stranded (ss) DNAs used in this study were purchased from Integrated DNA Technologies (Coralville, IA); azide-terminated and fluorescein-labeled ssDNA (F-ssDNA, 5'-/azide/ATGATGATGATGATGATG/FAM/-3'), capture ssDNA (5'-/azide/ATGATGATGATGATGATG/-3'), and linker ssDNA (5'-/GTTTGTTGTTGTTGGTAATTGTTG*TTTTTT*CATCATCATCATCATCAT/-3'; TMV 5' end complementary sequence *Spacer* capture ssDNA complementary sequence). Red fluorescent protein R-Phycoerythrin (R-PE in sodium phosphate buffer, pH 7.0 with ammonium sulfate) was purchased from AnaSpec (Fremont, CA).

Fabrication of Chitosan–PEG Microspheres

As shown in Figure 1a, chitosan–PEG microspheres were fabricated via a simple micromolding-based approach as in a recent study[1] with minor modifications. We first prepared a PDMS mold consisting of cross-shaped microwells with 5.14 nL of volume for large microspheres and with 1.20 nL for small

ones via thermal curing (overnight at 65 °C) of Sylgard 184 elastomer (9:1 weight ratio of elastomer to curing agent) on a photolithographically patterned silicon master mold. Next, we prepared aqueous prepolymer solutions by mixing chitosan (0.5% w/v), PEGDA (5-70% v/v) and deionized (DI) water, and hydrophobic wetting fluid by mixing *N*-hexadecane and PI (1% v/v). The prepolymer solution was placed on the PDMS mold, and filled into the microwells by rubbing the mold with a disposable pipet tip. The excess prepolymer solution was taken away by pipetting, and the filled mold was covered with the wetting fluid. These procedures were conducted in a humidity chamber with ~94% humidity to avoid rapid evaporation of water in the prepolymer solution.[2] The mold covered with the wetting fluid was left on an aluminum mirror (Thorlabs, Newton, NJ) for at least 2 min in order to form prepolymer droplets via surface tension at the interface between the prepolymer solution and the wetting fluid. Then, the droplets were exposed to 365 nm UV light with an 8 W hand-held UV lamp (Spectronics Corp., Westbury, NY) for 3 min in order to polymerize the droplets (i.e. crosslinking). The crosslinked droplets (i.e. microspheres) were collected by pipetting then washed 5 times with 2-propanol, 3 times with DI water containing 0.5% (v/v) TW20, and 2 times with 5× SSC buffer solution containing 0.05% (v/v) TW20 (SSC–TW20 buffer solution).

Swelling Ratio and Water Content of Chitosan–PEG Microspheres

The chitosan–PEG microspheres with varying PEG contents were immersed in SSC–TW20 buffer solution for at least 1 day to reach equilibrium swelling (i.e. wet state). The microspheres were then dried in a vacuum chamber at room temperature for at least 1 day upon washing 5 times with deionized water. The microspheres were imaged under a bright-field mode, and sphere diameters were analyzed with an image analysis software ImageJ[3] in order to compute the volumetric swelling ratio (γ):

$$\gamma = \frac{V_{wet}}{V_{dry}} \qquad \text{(S1)}$$

and water content:

$$\text{Water Content} = \frac{V_{wet} - V_{dry}}{V_{wet}} \times 100\% \qquad \text{(S2)}$$

where V_{wet} and V_{dry} represent sphere volumes under wet and dry states, respectively.

Preparation of Acrylate-modified Chitosans

To prepare acrylate-modified chitosans, some of chitosan's primary amines were replaced with acrylates by reacting 250 μL of 20 mg/mL chitosan in DI water with 20 μL of 100 mg/mL acrylate–PEG–SVA in DMSO (i.e. 2-fold molar excess over chitosan; ~7.4% molar ratio to the chitosan's

amines) for 2 h at room temperature. To separate the acrylate-modified chitosans from unreacted acrylate residues, the chitosans were precipitated by adding SSC–TW20 buffer solution (pH 7.0), then washed 3 times via centrifugation at 9000g for 30s with 500 μL of SSC–TW20 buffer solution. Note, soluble-insoluble transition of typical chitosans in aqueous solution arises between pH 6 and pH 6.5 due to their unique pKa value (~6.4).[4] Lastly, the pelleted acrylate-modified chitosans were dissolved in 250 μL of 0.1N HCl solution to prepare acrylate-modified chitosan solution (~2% w/v).

Fluorescent Labeling of Chitosan–PEG Microspheres

For fluorescent labeling of the chitosan–PEG microspheres prepared with acrylate-modified or unmodified chitosans, a constant number (~40) of the microspheres were incubated in SSC–TW20 buffer solution with 5 μM of NHS–fluorescein for 1 h at room temperature. The unreacted fluorescein residues were removed by washing the microspheres 3 times with aqueous solution containing 2-propanol (50% v/v).

TCO- or Azide-activation of Proteins

In order to activate R-PEs with TCO or azide molecules, we first exchanged buffer solution of the R-PE solution for borate buffered saline buffer solution (50 mM borate, 300 mM NaCl, pH 8.5) via centrifugal filtration at 4 ºC. The R-PEs (2 mg/mL) were then reacted with 20-fold molar excess of TCO–PEG_4–NHS ester or NHS–PEG_{12}–azide for 30 min at room temperature. Unreacted chemicals were separated from the R-PE solution via centrifugal filtration (Amicon Ultra 0.5) with PBS buffer solution (pH 7.4). Concentrations of the final R-PE solutions were measured by UV-vis spectrophotometry (Evolution™ 300 UV-vis Spectrophotometer, Thermo scientific, Waltham, MA) with the characteristic absorbance peaks and molar extinction coefficients of the R-PE[5] (1.96×10^6 $M^{-1}cm^{-1}$ at 565 nm).

Biomolecular Conjugation with Chitosan–PEG Microspheres

For biomolecular conjugation with the chitosan–PEG microspheres, we utilized Tz–TCO cycloaddition and strain-promoted alkyne–azide cycloaddition (SPAAC) reaction. First, the as-prepared chitosan–PEG microspheres were activated with Tz and ADIBO molecules upon incubation with 500 μM of Tz–PEG_5–NHS ester and ADIBO–*sulfo*–NHS ester in SSC–TW20 buffer solution for 1 h at room temperature, respectively. The unreacted chemicals were removed by washing the microspheres 4 times with SSC–TW20 buffer solution. To examine 3D network structures of the microspheres, the ADIBO-activated microspheres (~40 large-sized spheres) were reacted with 2 μM of azide-terminated F-ssDNAs and azide-activated R-PEs for 24 h in SSC–TW20 buffer solution at room temperature,

separately. To examine the effect of sphere size on protein conjugation capacity, a constant number (~120) of small ADIBO-activated microspheres were also reacted with 2 μM of azide-activated R-PEs for 24 h in SSC–TW20 buffer solution at room temperature. To examine protein conjugation kinetics with the microspheres, a constant number of (~120) small Tz- and ADIBO-activated microspheres were reacted with 2 μM of TCO- and azide-activated R-PEs for varying reaction times (0-48 h) in SSC–TW20 buffer solution at room temperature, respectively. The unconjugated biomolecules were separated from the microsphere solution by washing the microspheres 5 times with SSC–TW20 buffer solution.

Imaging Analysis

The fluorescently labeled, and F-ssDNA and R-PE conjugated microspheres were imaged with an epifluorescence microscope (Olympus BX51 equipped with a DP70 microscope digital camera, Center Valley, PA) and a confocal microscope (Leica DMIRE2 equipped with a TCS SP2 scanner, Wetzlar, Germany) in SSC–TW20 buffer solution (pH 7.0). Epifluorescence micrographs of the microspheres were obtained with a 10× objective under standard green (U-N31001) and red (U-N31002) filter sets (Chroma Technology Corp., Rockingham, VT) for the green fluorescent molecules (fluorescein and F-ssDNA) and the R-PEs, respectively. Confocal micrographs of the microspheres were obtained with a 20× objective at 488 nm and 543 nm excitation for the green fluorescent molecules and the R-PEs, respectively. Diameters and fluorescence intensities of the microspheres were analyzed with the image analysis software ImageJ.[3]

2. Core-shell Structure via Polymerization-induced Phase Separation

To confirm that the core-shell structure within microspheres in Figure 1c results from polymerization-induced phase separation (PIPS), we carried out comparison of apparent phase behavior with non-polymerizable system and that with polymerizable one, as shown in Figure S1. For the non-polymerizable systems, one of the components for polymerization is missing under identical fabrication conditions with that used in Figure 1; no photoinitiator (PI) in the wetting fluid (Figure S1a) and no acrylate in prepolymer solution (PEG200 instead of PEGDA, Figure S1b). For the polymerizable system, we utilized 30% PEGDA aqueous solution without chitosan as prepolymer solution (Figure S1c) to examine the effect of chitosan on the phase separation shown in Figure 1c. First, the bright-field micrographs in the top row of Figure S1 show uniform and transparent spherical droplets in both non-polymerizable and polymerizable systems upon surface tension-induced droplet formation, indicating no phase separation in the droplets before UV exposure. Next, UV-exposed droplets in the

polymerizable system (Figure S1c, bottom) clearly show two different phases (i.e. core-shell structure marked with long and short arrows) as shown in Figure 1c, while no core-shell structure is observed in the non-polymerizable systems upon UV exposure (Figure S1a,b bottom). These results indicate that polymerization of PEGDAs within the droplets, regardless of the chitosan, results in phase separation leading to formation of the core-shell structure in microspheres.

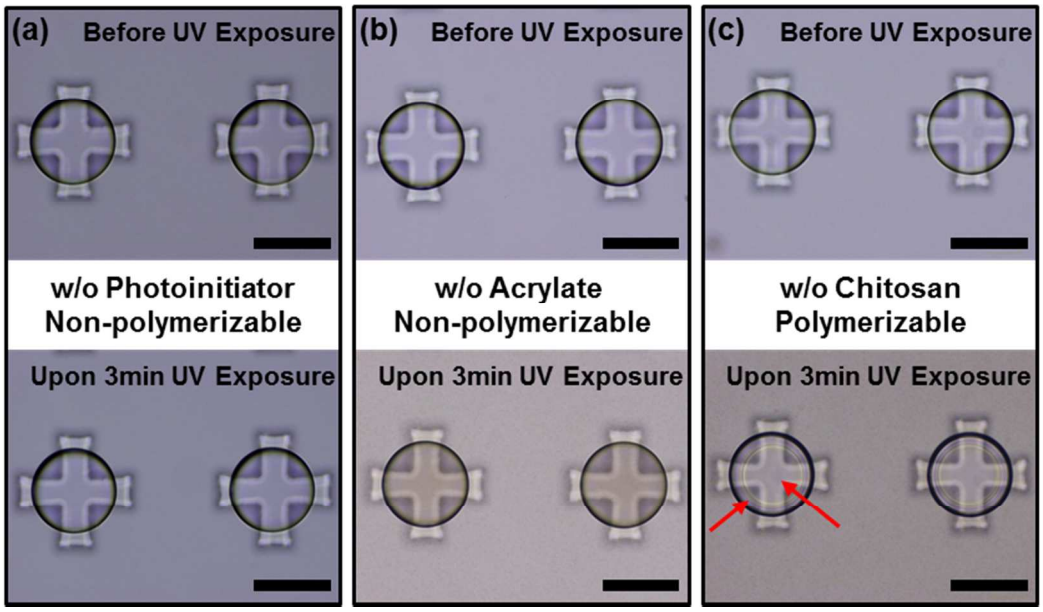

Figure S1. Bright-field micrographs of droplets before (top) and upon UV exposure (bottom). (a,b) Non-polymerizable systems; (a) without photoinitiators in the wetting fluid and (b) without acrylates in the prepolymer solution. (c) Polymerizable system without chitosans in the prepolymer solution. Long and short arrows indicate core and shell regions respectively. Scale bars represent 200 μm.

3. PEG-rich Core and PEG-poor Shell domains in Microspheres

We next examined the core-shell structure within microspheres shown in Figure 1 by utilizing binding affinity of a red fluorescent dye (sulforhodamine B, Sigma-Aldrich, St. Louis, MO) to PEG networks by hydrophobic adsorption,[6] as shown in Figure S2. For this, microspheres were fabricated with identical fabrication procedure and conditions as in Figure 1; surface tension-induced droplet formation of prepolymer solution consisting of 30% PEGDA and 0.5% chitosan upon addition of wetting fluid containing 1% PI, and 3 min UV exposure for polymerization. The microspheres were then washed with isopropanol (5 times), DI water with 0.5% TW20 (3 times) and 5xSSC buffer with 0.05% TW20 (2 times) sequentially, and incubated in an aqueous solution of sulforhodamine B (5 mg/mL in 5xSSC buffer with 0.05% TW20) for 3 h. Upon 3 times washing with the 5xSSC buffer with 0.05% TW20, the sulforhodamine B-adsorbed microspheres were analyzed with a confocal microscope (Leica

DMIRE2, Wetzlar, Germany). Specifically, the center plane of the microsphere was imaged with a 20× objective under transmitted light imaging mode (Figure S2a) and under 543 nm excitation (Figure S2b). First, the transmission mode (i.e. bright-field) confocal micrograph in Figure S2a clearly shows two different phases in the microsphere (i.e. core and shell regions marked with long and short arrows, respectively). Next, its corresponding fluorescence confocal micrograph (Figure S2b) shows significantly brighter fluorescence at the core region than the shell. We attribute this to more adsorbed dyes arising from higher polymer content,[6] or enhanced quantum yield of the dyes depending on specific microenvironment in a polymer matrix.[7] Regardless of the origin of the enhanced fluorescence at the core, this result indicates different network structure in each core and shell domain. Meanwhile, as shown in Figure S4, the results on the fluorescence of microspheres with varying PEG contents through nonspecific adsorption clearly indicate increase in fluorescence with increasing PEG contents of the microspheres. Combined with this result, the result in Figure S2 showing different network structure in each core and shell suggests variation of PEG content in each domain; the microspheres in Figure 1 are composed of PEG-rich core and PEG poor shell.

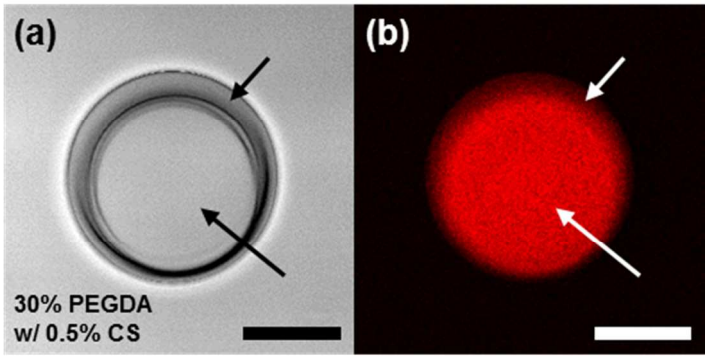

Figure S2. Confocal micrographs at the center plane of the sulforhodamine B-adsorbed microsphere under (a) transmitted light imaging mode and (b) 543 nm excitation. Long and short arrows indicate core and shell regions respectively. Scale bars represent 100 μm.

4. Chitosan–PEG Microspheres under Wet and Dry States

As shown in Figure S3, we fabricated microspheres with prepolymer solutions containing varying concentrations of PEGDA (10-50% v/v) and fixed amount of chitosan (0.5% w/v) in order to examine the effect of PEGDA concentration on swelling of the microspheres (Figure 1e). The bright-field micrographs in Figure S3a-c show representative microspheres prepared with varying PEGDA concentrations under wet (swollen, top) and dry (shrunken, bottom) states. The results show that both wet and dry microspheres are highly uniform for all PEGDA concentrations examined, indicating consistent microsphere fabrication with our simple micromolding-based technique. The difference in

sphere size between wet and dry states (i.e. degree of swelling) decreases with increasing PEGDA concentration due to varying crosslinking densities and polymer contents resulting from the PEGDA concentrations.[8, 9] Note that the wet 10% PEGDA spheres are more transparent than the 30% and 50% PEGDA ones, due to lower PEG content.

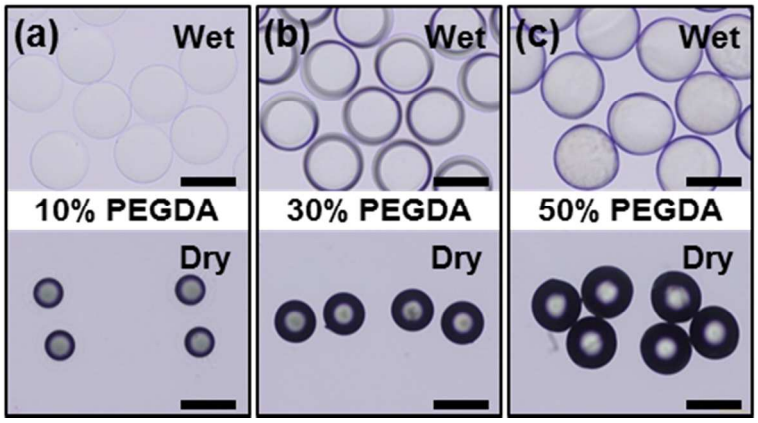

Figure S3. Representative bright-field micrographs of the microspheres fabricated with varying PEGDA concentrations under wet (top row) and dry states (bottom row); (a) 10%, (b) 30%, and (c) 50% PEGDA. Scale bars represent 200 μm.

Note that, our micromolding-based method allows substantially low polymer content microstructures to be readily fabricated with retained mechanical integrity and uniform shape (down to 5% PEGDA microspheres, data not shown), which is challenging with other methods (e.g. PDMS-based replica molding technique[10] and stop-flow lithography[11]). We attribute this to less oxygen-inhibited environment for the radical polymerization (i.e. less severe radical scavenging by oxygen) in our system than the PDMS-based ones; dissolved oxygen in the wetting fluid (one order of magnitude smaller amount than the dissolved PIs, based on solubility of oxygen in *N*-hexadecane[12]) will be rapidly consumed by radicals generated from UV-exposed PIs with the high consumption rate constant ($\sim 10^8$ $M^{-1}s^{-1}$),[13] allowing for prevention of oxygen supply to the droplets during the polymerization. In contrast, the dissolved oxygen in the PDMS-based systems continuously diffuse in through the permeable PDMS layers, and inhibit the polymerization by scavenging the radicals.[13] Additionally, the abundant PIs in the wetting fluid along with long UV exposure time (i.e. several minutes versus milliseconds in the stop-flow lithography[11]) should allow the microspheres to be fully polymerized, leading to well-defined microstructures with low polymer content. Meanwhile, convenience of our simple batch processing-based micromolding setup allows for a wide range of polymerization reaction parameters (e.g. UV exposure time and PI concentration) to be readily employed and tuned.

5. Minimal Fluorescence of Microspheres without Chitosan

In order to confirm that the observed fluorescence on the chitosan–PEG microspheres in Figure 2 is due to the specific S_N2 reaction between NHS–fluorescein molecules and chitosan's primary amines, we carried out negative control experiments with microspheres where chitosan is missing, as shown in Figure S4. Specifically, the microspheres were fabricated with prepolymer solutions consisting of 10-70% PEGDA without chitosan, and incubated in aqueous solutions containing 5μM of NHS–fluorescein for 1 h. Upon 3 times washing, the microspheres were imaged with epifluorescence microscopy under identical imaging conditions as in Figure 2.

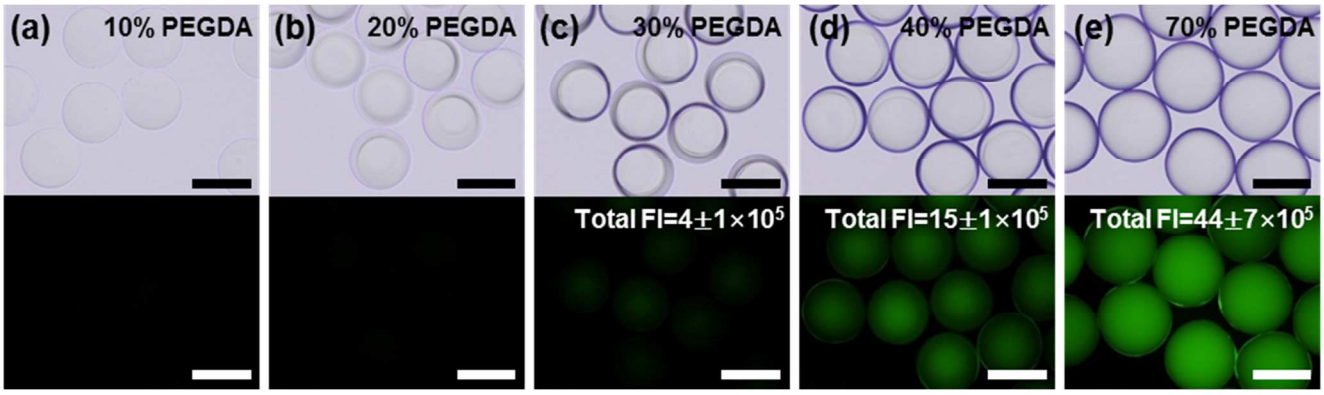

Figure S4. Bright-field (top row) and fluorescence micrographs (bottom row) of microspheres without chitosan upon incubation in an aqueous solution of NHS–fluorescein; microspheres fabricated with prepolymer solution containing (a) 10% (v/v), (b) 20% (v/v), (c) 30% (v/v), (d) 40% (v/v) and (e) 70% (v/v) PEGDA without chitosan. Scale bars represent 200 μm.

As shown in the bright-field micrographs (Figure S4a-e, top row), the microspheres are uniform for all the PEGDA concentrations employed as in Figure 2, indicating consistency and robustness of our simple micromolding-based fabrication method. Next, the fluorescence micrographs corresponding to the bright-field ones (Figure S4a-e, bottom row) show no fluorescence on the microspheres prepared with 10-20% PEGDA, indicating minimal nonspecific binding of fluorescein with the microspheres. While microspheres prepared with 30-70% PEGDA show some fluorescence that increases with the PEGDA concentration, the average total fluorescence is substantially lower than the microspheres with chitosan shown in Figure 2; one order of magnitude lower average total fluorescence on the microspheres without chitosan (total FI=10^5-10^6) than that with chitosan (total FI=10^6-10^7) for every PEGDA condition examined. We attribute this fluorescence on higher PEG content microspheres to hydrophobic adsorption of the fluorescein to the PEG residues, similar to the binding of sulforhodamine B to the PEG networks shown in Figure S2. In the meantime, highly hydrophilic

nature of chitosan leads to negligible nonspecific binding with fluorescein,[14] supporting specific conjugation of the fluorescein molecules with the chitosan's amines via the S_N2 reaction. The low fluorescence on the microspheres without chitosan shown in Figure S4 confirms that most of the fluorescence on the chitosan–PEG microspheres in Figure 2 results from covalently conjugated fluorescein molecules via the specific S_N2 reaction.

6. Microspheres Fabricated with Acrylate-modified Chitosan

As shown in Figure S5, we further examined the distribution of chitosan and the polymerization-induced phase separation (PIPS) using acrylate-modified chitosan. We hypothesized that the acrylate–chitosan should be more efficiently copolymerized with PEGDA than the unmodified chitosan, enhancing the incorporation ratio and suppressing the mobility of chitosan moieties during the PIPS. To prepare the acrylate–chitosan, small portions of the chitosan's amines were replaced with acrylates via S_N2 reaction using 2-fold molar excess of amine-reactive acrylate–PEG–succinimidyl valerate over chitosan (i.e. ~7.4% molar ratio to chitosan's amines). The microspheres fabricated with the acrylate–chitosan and PEGDA were analyzed under identical fabrication and imaging conditions as in Figure 2.

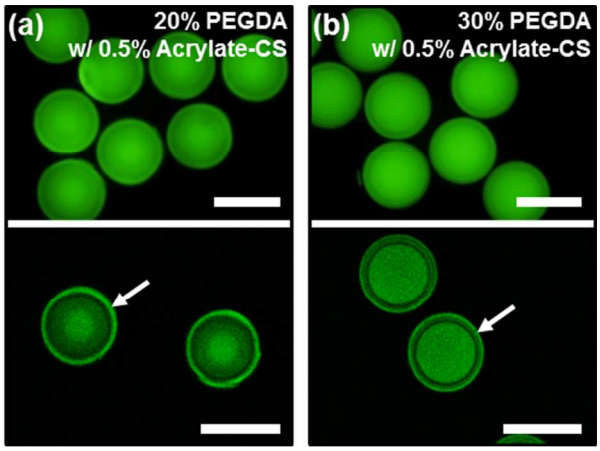

Figure S5. Chitosan distribution in microspheres fabricated with acrylate–chitosan. (a,b) Fluorescence (top row) and confocal micrographs (bottom row) of (a) 20% and (b) 30% PEGDA microspheres fabricated with 0.5% acrylate–chitosan. All scale bars represent 200 μm.

First, the fluorescence micrographs of the microspheres fabricated with the acrylate–chitosan (Figure S5a,b, top row) show relatively uniform fluorescence throughout the microspheres in contrast to those with the unmodified chitosan showing core-shell like fluorescence distribution (Figure 2c,d), suggesting suppressed migration of chitosan moieties during polymerization. Next, the confocal micrographs at the particle centers (Figure S5a,b, bottom row) show a bright fluorescent layer near the

sphere surfaces (marked with arrows) as well as core-shell like fluorescence distribution, unlike the results in Figure 2c,d (i.e. dim fluorescence near the surface). This result suggests that the acrylate–chitosan is copolymerized with the PEGDA near the droplet surfaces at the onset of the polymerization, then subsequently localized and copolymerized with the PEGDA that is pushed into the core area via the PIPS. In summary, the results with acrylate-modified chitosan in Figure S5 show that copolymerization of chitosan moieties with PEGDAs suppresses migration of the chitosan moieties, further supporting PIPS-based formation of core-shell structures.

7. Apparent Chitosan Incorporation Ratio

As shown in Figure S6, we next carried out total fluorescence intensity analysis for the fluorescently labeled microspheres fabricated with unmodified and acrylate-modified chitosan in order to compare the incorporation ratio of both types of chitosan for a range of PEGDA concentrations. For this, the average total fluorescence intensity was analyzed via an image analysis software (ImageJ)[3] with four randomly selected microspheres for each case. First, the total fluorescence intensity plot for both types of microspheres (with unmodified chitosan, open circles & with acrylate–chitosan, open squares in Figure S6a) show increase in fluorescence intensity (i.e. chitosan incorporation) with increasing PEGDA concentration, presumably due to combination of higher polymerization efficiency (i.e. more number of acrylates) and small mesh size at higher PEGDA content conditions.[10, 11] Particularly, the acrylate–chitosan particles at 10% PEGDA show higher fluorescence intensity than those with the unmodified chitosan, indicating improved chitosan incorporation due to more efficient copolymerization of the acrylate–chitosan with the PEGDA. In the meantime, the acrylate–chitosan particles for 20-40% PEGDA range show lower fluorescence intensity values than those with unmodified chitosan, presumably due to the reduced number of chitosan's reactive amines from the acrylate modification step (i.e. NHS ester reaction with amines), rather than to lower chitosan incorporation. Meanwhile, irregular fluorescence on the microspheres with the acrylate–chitosan (i.e. aggregated chitosan, similar to Figure 2f; 60-70% PEGDA) is observed at 50% PEGDA composition resulting from incompatibility of chitosan and PEGDA in the prepolymer solution (possibly due to higher polymer contents from the PEG–acrylate chains on the chitosan backbone, data not shown).

Next, we evaluated apparent chitosan incorporation ratio (η, table of Figure S6b) by normalization with the fluorescence intensity of 50% PEGDA microspheres, where the chitosan incorporation should be maximal among the conditions examined due to sufficient number of PEGDA's acrylates for the amine-radical reaction.[10] First, 10% PEGDA condition shows 2.6-fold enhancement in the apparent chitosan incorporation for the acrylate–chitosan. Next, assuming that all the acrylate–chitosan

moieties in the droplets at 40% PEGDA are incorporated due to covalent linkage and/or physical entrapment,[11] the apparent chitosan incorporation ratio with the acrylate–chitosan (η=0.58) suggests that ~42% of the amines on the chitosan backbone are unavailable for further amine-reactive reactions presumably due to reduced accessibility of the amines by grafted chains as well as their consumption in the acrylate modification step (max. ~7.4% based on molar ratio employed here). Accounting for this reduced amine titer, the maximum incorporation ratio of the acrylate–chitosan at 10% PEGDA should be ~45% (corrected η≈0.45); i.e. 4.5-fold enhanced incorporation with the acrylate–chitosan over that with the unmodified chitosan.

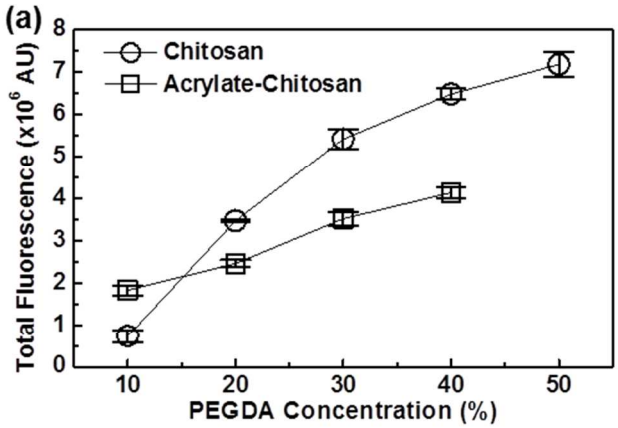

(b) Apparent Chitosan Incorporation Ratio (η)

PEGDA [%]	10	20	30	40	50
Chitosan	0.10	0.48	0.75	0.90	1.0
Acrylate-Chitosan	0.26	0.34	0.49	0.58	-

Figure S6. Comparison of incorporation ratio between unmodified chitosan and acrylate–chitosan. (a) Average total fluorescence intensity plots of the microspheres with unmodified chitosan (open circles) and acrylate–chitosan (open squares). Error bars represent standard deviation from five microspheres per each condition. (b) Table for summary of calculated apparent chitosan incorporation ratios based on total fluorescence intensities in (a).

8. Compatibility of Chitosan with PEGDA in Aqueous Solution

Figure S7 shows the effect of PEGDA concentration on compatibility of chitosan with PEGDA in aqueous prepolymer solutions. For this, we prepared 500 μL of aqueous prepolymer solutions by mixing fixed amount of chitosan (0.5% w/v) with varying concentrations of PEGDA (10-70% v/v), and examined turbidity of the prepolymer solution's absorbance at 450 nm (Abs_{450}) with an Evolution™ 300 UV-vis Spectrophotometer (Thermo scientific, Waltham, MA) at room temperature. As shown in

Figure S7, the prepolymer solutions containing up to 50% PEGDA are clear (i.e. Abs_{450}≈0), indicating compatible composition of the prepolymer solutions (i.e. one-phase). The prepolymer solutions then become turbid above 60% PEGDA composition, showing increasing Abs_{450} with increasing PEGDA concentration. This result indicates that the chitosan is incompatible with PEGDA in the prepolymer solutions containing PEGDA above 60%, forming aqueous two-phase system with the hydrophilic chitosan undergoing phase separation from more hydrophobic PEGDA-rich phase.[15] This phase behavior likely leads to the observed uniform fluorescence of chitosan–PEG microspheres with lower PEG content (Figure 2b-e), and the bright fluorescence of the aggregated chitosan and minimal fluorescence elsewhere for the high PEG content microspheres (Figure 2f). In other words, the bright fluorescence of the aggregated phase in high PEG content microspheres in Figure 2f likely resulted from the phase-separation of chitosan in the prepolymer solution that remains chemically active for labeling with NHS–fluorescein.

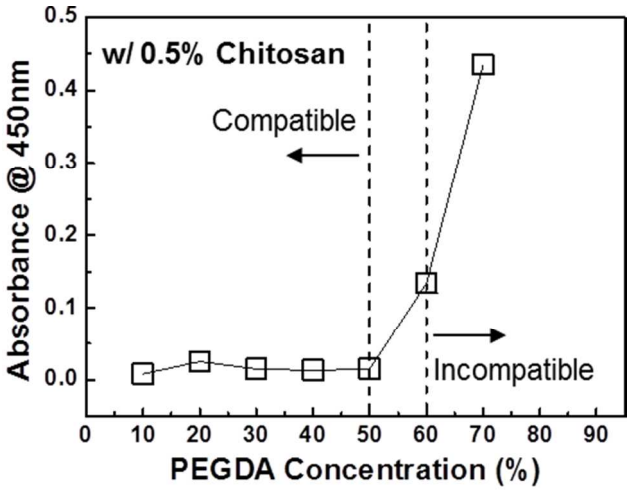

Figure S7. Phase diagram of the aqueous prepolymer solution composed of varying concentrations of PEGDA (10-70% v/v) and fixed amount of chitosan (0.5% w/v).

9. Negligible Biomolecular Conjugation with High PEG Content Microspheres

As shown in Figure S8, we also carried out biomolecular conjugation with high PEG content (40% PEGDA) microspheres via SPAAC reaction as in Figure 3. Upon ADIBO activation and conjugation reaction with azide-modified biomolecules (i.e. F-ssDNA and R-PE) via SPAAC reaction, the fluorescence micrographs of the microspheres (Figure S8a,b, top row) show negligible fluorescence, similar to non-fluorescence on the microspheres missing ADIBO-activation (Figure S8a,b, bottom row). This result indicates that both F-ssDNA and R-PE are minimally conjugated with the microspheres due to small mesh size of the high PEG content microspheres despite high chitosan

incorporation (Figure S6), leading to mass transfer limitation of the relatively large biomolecules into the microspheres.[10, 16]

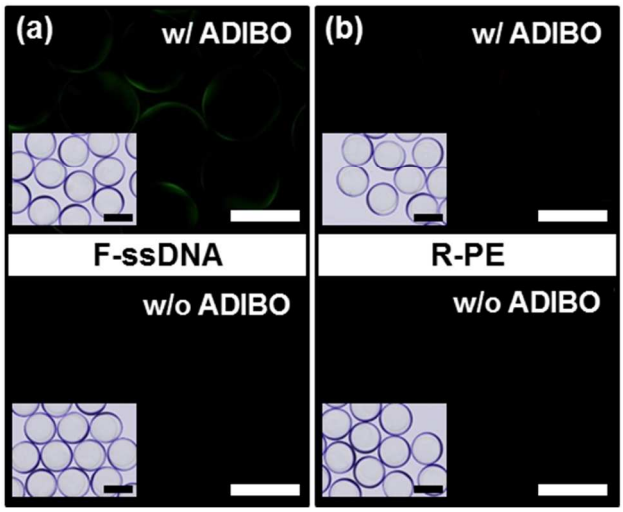

Figure S8. Fluorescence micrographs of 40% PEGDA microspheres with and without ADIBO-activation (top and bottom rows respectively) upon incubation with (a) F-ssDNAs and (b) R-PEs. Insets are bright-field micrographs corresponding to each fluorescence micrograph. All scale bars represent 200 μm.

10. TMV Assembly with Microspheres

As shown in Figure S9, we further examined the mesh size of the 10-20% PEGDA microspheres (i.e. entire 10% PEGDA microspheres and the shell layers of 20% PEGDA ones, Figure 3) by utilizing significantly large supramolecules, nanotubular tobacco mosaic virus (TMV, 18×300 nm dimension and hydrodynamic radius R_h≈55 nm[17]). For this, we exploited hybridization-based TMV-assembly approach,[18] following the procedures described in our recent study[19] (schematic diagram of Figure S9a). Briefly, 300 μg/mL of genetically modified TMV[18] (TMV1cys) was fluorescently labeled; 2 h incubation at room temperature in an aqueous solution (100 mM sodium phosphate buffer, pH 7.0) containing 10-times molar excess of fluorescein–5–maleimide over the cysteines that are genetically displayed on the surface of the TMV1cys. The TMVs were then purified from unreacted fluorescein residues and partially disassembled to expose their 5'-end mRNA sequence via ultracentrifugation (at 48000g for 2 h) in a 10-40% sucrose gradient (100 mM Tris buffer, pH 7.5). Next, the fluorescently labeled and partially disassembled TMVs were purified (i.e. pelleted with ultracentrifugation at 90000g for 1 h, then resuspended in 5×SSC buffer solution), and hybridized with linker single-stranded (ss) DNAs (10:1 molar ratio to the TMV) whose sequence consists of two different regions complementary to TMV's 5′-end mRNA and to the capture ssDNA (conjugated with

the microspheres via SPAAC reaction, Materials and Methods). Lastly, these TMVs were incubated with the capture ssDNA-conjugated microspheres for 24 h at 30 ºC to assemble the TMVs with the microspheres via nucleic acid hybridization. The TMV-assembled microspheres were then analyzed via epifluorescence and confocal microscopy.

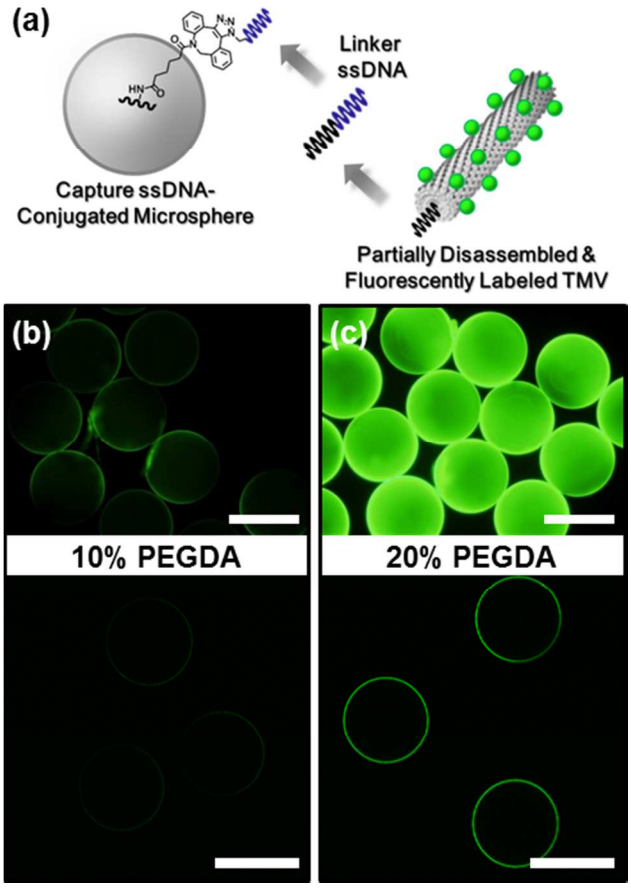

Figure S9. Assembly of tobacco mosaic virus (TMV) with the chitosan–PEG microspheres via nucleic acid hybridization. (a) Schematic diagram for hybridization-based assembly of fluorescein-labeled and partially disassembled TMV with capture ssDNA-conjugated microspheres. (b,c) Fluorescence (top row) and confocal (bottom row) micrographs of TMV-assembled microspheres fabricated with (b) 10% PEGDA and (c) 20% PEGDA. All scale bars represent 200 μm.

First, the epifluorescence micrographs (Figure S9b,c, top row) show distinguishable fluorescence (brighter fluorescence near surfaces) on both 10% and 20% PEGDA microspheres indicating assembled TMVs, similar to our previous study.[10] Total fluorescence on the 20% PEGDA microspheres is brighter than that on the 10% PEGDA ones. Next, the confocal micrographs (Figure S9b,c, bottom row) show very thin fluorescence layers (roughly 1 μm) at the surfaces of both microspheres, consistent with the epifluorescence results. This result illustrates that the mesh size of

the macroporous regions in the 10-20% PEGDA microspheres are not large enough for penetration of the TMVs (R_h≈55 nm), and the TMVs are assembled only at the sphere surfaces. Meanwhile, brightness of the fluorescence layer on the 20% PEGDA microspheres is higher than that on the 10% PEGDA ones, consistent with the epifluorescence results (Figure S9b,c, top row). We attribute this brighter fluorescence to higher surface density of the capture ssDNAs on the 20% PEGDA microspheres, enabling the TMVs to be assembled at the sphere surfaces in higher density. In short summary, the results in Figure S9 combined with the penetration results for R-PEs (R_h≈5.6 nm) in Figure 3 suggest quite uniform mesh size through macroporous regions in 10-20% PEGDA microspheres; larger than the size of R-PE (R_h≈5.6 nm) and smaller than the size of TMV (R_h≈55 nm).

11. Size-selective Dual Conjugation with Core-shell Structured Microspheres

As shown in Figure S10, we demonstrate size-selective conjugation of red fluorescent protein (R-PE, MW 240 kDa) and green fluorescent marker (F-488, MW 576 Da) with core-shell structured chitosan–PEG microspheres via SPAAC reaction. Specifically, the core-shell structured microspheres were fabricated with 20% PEGDA as in Figure 2c and 3c,f, and activated with ADIBO molecules (500 μM of ADIBO–*sulfo*–NHS ester) for 30 min at room temperature. The ADIBO-activated microspheres were then incubated with 2 μM of azide-activated R-PE in 5× SSC buffer solution with 0.05% (v/v) TW20 (SSC–TW20) for 6 h. Upon washing, the R-PE conjugated microspheres were incubated with 2 μM of azide-containing F-488 for 12 h in aqueous solution (SSC–TW20 with 4% (v/v) DMSO) at room temperature. The microspheres conjugated with both fluorescent molecules were imaged at the center plane with a confocal microscope under 543 nm and 488 nm excitation for the R-PE and the F-488, respectively.

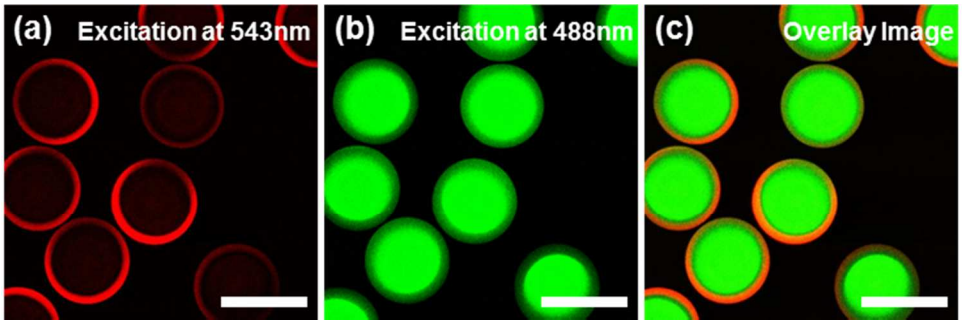

Figure S10. Size-selective conjugation of red fluorescent protein R-phycoerythrin (R-PE, MW 240 kDa) and green fluorescent marker (F-488, MW 576 Da) with core-shell structured chitosan–PEG microspheres. (a,b) Confocal micrographs of the core-shell microspheres conjugated with the R-PE and F-488; excitation at (a) 543 nm and (b) 488 nm. (c) Overlay image of (a) and (b). All scale bars represent 200 μm.

The confocal micrographs show red fluorescence near the sphere surfaces (Figure S10a), and bright green fluorescence around the cores (Figure S10b). This result indicates that the large R-PEs are conjugated only at the well-defined macroporous shell layers (consistent with the result in Figure 3f), and that the small F-488 molecules pass through the R-PE conjugated shell layers then are conjugated around the cores. The overlay image (Figure S10c) of the confocal micrographs more clearly shows distinct R-PE conjugated shell and F-488 conjugated core regions. Combined, the results in Figure S10 show size-selective conjugation that allows different molecules to be placed with spatial control (i.e. core and shell) in the microspheres even using the same conjugation reaction (i.e. SPAAC). This suggests potential for programmable functionalization of our core-shell microspheres by utilizing multiple functionalities of varying sizes. For example, large antibodies with cell- or surface ligand-specificity can be conjugated at and near the sphere surfaces for targeting, while the remaining and abundant (ADIBO-activated) chitosan sites can be loaded with small therapeutic drug molecules for targeted drug delivery applications.[20]

12. Effect of Sphere Size on Protein Conjugation Kinetics

As shown in Figure S11, we compared protein conjugation kinetics behavior between the large and small microspheres via SPAAC reaction. For this, we prepared large (204 μm and 209 μm diameter) and small (131 μm and 133 μm diameter) 10-20% PEGDA microspheres, and activated them with ADIBO molecules via S_N2 reaction with 500 μM of ADIBO–*sulfo*–NHS ester for 1 h at room temperature. These microspheres were then reacted with 2 μM of azide-activated R-PEs for 0-48 h at room temperature. Average total fluorescence intensity of the R-PE conjugated microspheres were analyzed with an image analysis software ImageJ.[3] First, the total fluorescence plots of the large microspheres (open squares and circles) show gradual increase in fluorescence with time, approaching saturation toward the end of the 48 h reaction period. Total fluorescence intensity of the small microspheres (solid squares and circles) also gradually increases with time, yet reaches near-saturation upon 24 h reaction. These results indicate that larger microspheres take longer time to be fully conjugated with the R-PEs resulting from longer diffusion length. In other words, the protein conjugation kinetics behavior with the microspheres appears to be governed by diffusion of the proteins through the microspheres under the reaction conditions enlisted here (further discussed in Figure 5). Meanwhile, the difference in protein conjugation capacity between the large and small microspheres upon 48 h reaction (~4 times larger capacity of the large microspheres) is equivalent to their difference in volume (roughly 4-fold larger volume). Assuming that the reaction approaches completion in the 48 h period, this result suggests that maximum protein conjugation capacity of the

microspheres is directly proportional to their volume, and that the 3D network structures of the microspheres (i.e. chitosan incorporation ratio and mesh size) and the availability of reactive ADIBO sites (thus chitosan) should be consistent for various sphere sizes.

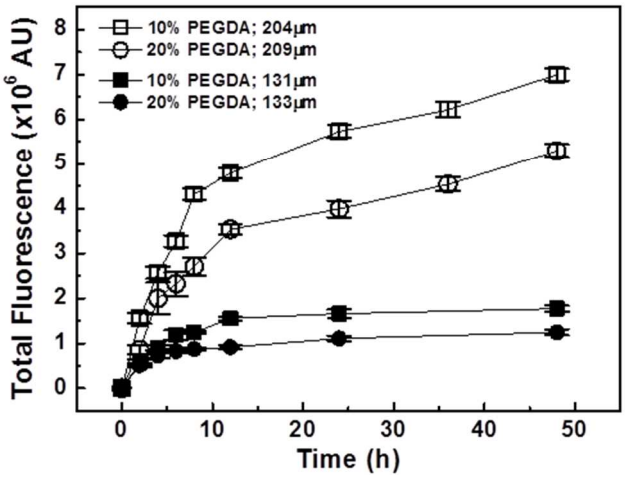

Figure S11. R-PE conjugation kinetics with different-sized microspheres via SPAAC reaction for 48 h. Small microspheres; 131 μm and 133 μm diameters (solid squares and circles respectively), and large microspheres; 204 μm and 209 μm diameters (open squares and circles respectively). Error bars represent standard deviation from five microspheres per each condition.

13. Estimated Number of Conjugation Sites in Microspheres

To examine our hypothesis on abundant protein conjugation sites in the small (131 μm diameter) 10% PEGDA microspheres, the number of conjugation sites was estimated, and compared with the maximum number of R-PEs that can be packed in the microsphere, as shown in Figure S12. First, since the chitosan's primary amines in the microsphere are activated with ADIBO molecules for protein conjugation, we estimated the number of primary amines as the conjugation sites by utilizing chitosan incorporation ratio (Figure S12a). The chitosan incorporation results (Figure S6b) show that ~10% of chitosans (η=0.1) in the prepolymer droplet are incorporated in the large 10% PEGDA microspheres, and the result in Figure S11 suggests this incorporation ratio is also retained in the small ones. The droplet volume is equivalent to that of the micromold (V_M=1.20 nL for small microspheres). Thus, the number of incorporated chitosans in the small 10% PEGDA microsphere can be estimated as follows:

$$N_{CS} = V_M \times C_{CS} \times \eta \times \frac{1}{MW_{CS}} = 1.20\ \text{nL} \times \frac{0.5\ \text{g}}{100\ \text{mL}} \times 0.1 \times \frac{\text{moles}}{5000\ \text{g}} = 1.20\ \times 10^{-13}\ \text{moles}$$

where C_{CS} and MW_{CS} represent concentration (0.5% w/v) and molecular weight (5 kDa) of the chitosan in the droplet, respectively.

The number of the primary amines per chitosan with 90% deacetylation is:

$$n_{Am} = \frac{MW_{CS}}{MW_{R-CS}} \times 0.9 = \frac{5000}{161} \approx 27$$

where MW_{R-CS} represents molecular weight (161 Da) of the glucosamine repeating unit of the chitosan.

Thus, the number of the primary amines (i.e. conjugation sites) in the microsphere is:

$$\underline{\boldsymbol{N_{Am}}} = N_{CS} \times n_{Am} = \underline{\mathbf{3.24 \times 10^{-12}\ moles}}$$

We note that not all of these conjugation sites should be equally accessible for the protein conjugation partly due to steric hindrance resulting from multiple amines existing in a close proximity on a chitosan backbone.

Next, we estimated the maximum number of R-PEs that can be packed in the microsphere with assumptions that the R-PEs are hard spheres with 5.6 nm radius[21] (i.e. hydrodynamic radius), and densely packed in a face-centered cubic (FCC) structure. To simplify this estimation, we also assume that the number of the packed R-PEs in the microsphere is equivalent to that in an imaginary cube whose volume is the same with that of the microsphere (Figure S12b).

The volume of the microsphere and also the imaginary cube is:

$$V_{SP} = V_{IC} = \frac{4}{3} \times \pi \times {r_{SP}}^3 = 1.18 \text{ nl}$$

where r_{SP} represents radius (65.6 μm) of the microsphere.

The FCC unit cell volume consisting of four R-PEs[22] is:

$$V_{FCC} = 16 \times {r_{R-PE}}^3 \times \sqrt{2} = 3.97 \times 10^{-12} \text{ nl}$$

where r_{R-PE} represents radius (5.6 nm) of the R-PE.

Thus, the maximum number of R-PEs packed via FCC configuration in the imaginary cube (i.e. microsphere) is:

$$\underline{\boldsymbol{N_{R-PE}}} = \frac{V_{IC}}{V_{FCC}} \times 4 \times \frac{\text{moles}}{6.02 \times 10^{23}} = \underline{\mathbf{1.97 \times 10^{-12}\ moles}}$$

We note that this value is an estimated one under ideal conditions (i.e. tightly packed in the empty space). In other words, the number of R-PEs conjugated in the microsphere should be much less than this estimated maximum value due to excluded volume in the microsphere by polymer networks and the R-PEs conjugated along the incorporated chitosans rather than tightly packed.

Overall, the estimation results in Figure S12 show that a 10% PEGDA microsphere could possess roughly 1.6-fold more conjugation sites (i.e. chitosan's amines) than the maximum number of R-PEs that can be packed in the microsphere under ideal conditions. This suggests that there exist sufficient sites for protein conjugation in the microsphere, while the sites may not be equally available or accessible due to steric hindrance.

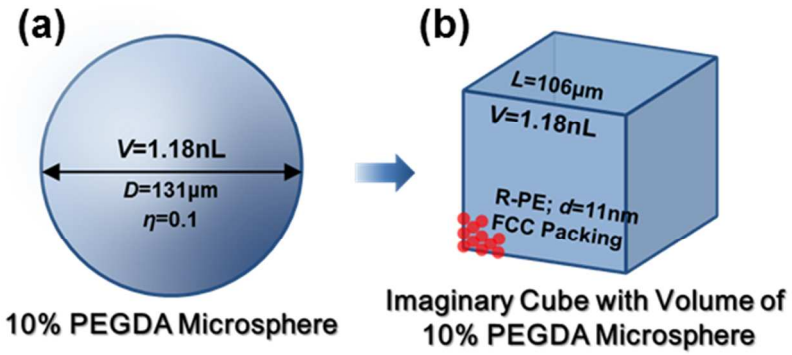

Figure S12. Schematic diagrams of (a) the 10% PEGDA microsphere, and (b) an imaginary cube possessing the same volume with the 10% PEGDA microsphere and filled with the R-PEs in compact face-centered cubic (FCC) structure.

References

(1) Choi, C. H.; Jeong, J. M.; Kang, S. M.; Lee, C. S.; Lee, J. *Adv. Mater.* **2012**, *24*, 5078.

(2) Lewis, C. L.; Choi, C. H.; Lin, Y.; Lee, C. S.; Yi, H. *Anal. Chem.* **2010**, *82*, 5851.

(3) Rasband, W. S. *Imagej*; U. S. National Institutes of Health: Bethesda, MD, 1997-2012.

(4) Yi, H.; Wu, L. Q.; Bentley, W. E.; Ghodssi, R.; Rubloff, G. W.; Culver, J. N.; Payne, G. F. *Biomacromolecules* **2005**, *6*, 2881.

(5) AnaSpec Anaspec, Inc. Home Page. http://www.anaspec.com/products/product.asp?id=29041 (accessed January).

(6) Guo, S.; Yao, T.; Ji, X. B.; Zeng, C. F.; Wang, C. Q.; Zhang, L. X. *Angew. Chem. Int. Ed.* **2014**, *53*, 7504.

(7) Hodgson, R. J.; Plaxton, W. C. *FEBS Lett.* **1995**, *368*, 559.

(8) Pacios, I. E.; Molina, M. J.; Gomez-Anton, M. R.; Pierola, I. F. *J. Appl. Polym. Sci.* **2007**, *103*, 263.

(9) Reinhart, C. T.; Peppas, N. A. *J. Membr. Sci.* **1984**, *18*, 227.

(10) Jung, S.; Yi, H. *Langmuir* **2012**, *28*, 17061.

(11) Pregibon, D. C.; Doyle, P. S. *Anal. Chem.* **2009**, *81*, 4873.

(12) Ju, L. K.; Ho, C. S. *Biotechnol. Bioeng.* **1989**, *34*, 1221.

(13) Dendukuri, D.; Panda, P.; Haghgooie, R.; Kim, J. M.; Hatton, T. A.; Doyle, P. S. *Macromolecules* **2008**, *41*, 8547.

(14) Yi, H.; Wu, L. Q.; Sumner, J. J.; Gillespie, J. B.; Payne, G. F.; Bentley, W. E. *Biotechnol. Bioeng.* **2003**, *83*, 646.

(15) Kaul, A. The Phase Diagram. In *Methods in Biotechnology*; Hatti-Kaul, R., Ed.; Humana Press: Totowa, NJ, 2000; Vol. 11.

(16) Jung, S.; Yi, H. *Biomacromolecules* **2013**, *14*, 3892.

(17) Santos, N. C.; Castanho, M. A. R. B. *Biophys. J.* **1996**, *71*, 1641.

(18) Yi, H.; Nisar, S.; Lee, S. Y.; Powers, M. A.; Bentley, W. E.; Payne, G. F.; Ghodssi, R.; Rubloff, G. W.; Harris, M. T.; Culver, J. N. *Nano Lett.* **2005**, *5*, 1931.

(19) Jung, S.; Yi, H. *Langmuir* **2014**, *30*, 7762.

(20) Fahmy, T. M.; Fong, P. M.; Goyal, A.; Saltzman, W. M. *Mater. Today* **2005**, *8*, 18.

(21) Goulian, M.; Simon, S. M. *Biophys. J.* **2000**, *79*, 2188.

(22) Callister, W. D. *Materials Science and Engineering: An Introduction*; John Wiley & Sons, Incorporated: Hoboken, NJ, 2006.